

Normal State Nernst Effect in Electron-doped $\text{Pr}_{2-x}\text{Ce}_x\text{CuO}_{4-\delta}$: Superconducting Fluctuations and Two-band Transport

Pengcheng Li* and R. L. Greene

Center for Superconductivity Research and Department of Physics,
University of Maryland, College Park, Maryland 20742-4111, USA

(Dated: September 20, 2021)

We report a systematic study of normal state Nernst effect in the electron-doped cuprates $\text{Pr}_{2-x}\text{Ce}_x\text{CuO}_{4-\delta}$ over a wide range of doping ($0.05 \leq x \leq 0.21$) and temperature. At low temperatures, we observed a vortex Nernst signal well above T_c in the underdoped films, but no such normal state vortex Nernst signal is found in the overdoped region. The superconducting fluctuations in the underdoped PCCO are compatible with incoherent phase fluctuations. At high temperatures, a large normal state Nernst signal is found at dopings from slightly underdoped to highly overdoped. Combined with normal state thermoelectric power, Hall effect and magnetoresistance measurements, the large Nernst effect is compatible with two-band model. For the highly overdoped films, the large Nernst effect is anomalous and not explainable with a simple hole-like Fermi surface seen in photoemission experiments.

PACS numbers: 74.25. Fy, 74.40. +k, 74.72. Jt

I. INTRODUCTION

The anomalously large Nernst voltage well above the zero-field T_c in hole-doped cuprate superconductors is now a well established experimental observation with a dominant view that it is due to vortex-like excitations above T_c .^{1,2} The appearance of the Nernst signal on approaching T_c from above marks the onset of a phase uncorrelated pairing amplitude. The observation of an enhanced diamagnetism near the onset temperature T_ν of the anomalous Nernst signal in some hole-doped cuprates strongly supports the vortex-like excitations scenario.¹ The fact that the regime of this large Nernst effect overlaps with the temperature range where a pseudogap is seen in the electronic excitation spectrum, also suggests that the anomalous Nernst effect is related to the pseudogap phenomenon.

Inspired by the unusual Nernst effect measurements in hole-doped cuprates, many theories to explain these striking observations have been proposed. Two of these theories deal with amplitude and phase fluctuations of the superconducting order parameter. Ussishkin *et al.*⁴ suggest that Gaussian amplitude fluctuations above T_c are responsible for the Nernst effect for the optimally-doped and overdoped regimes. For the underdoped regime they suggest that strong non-Gaussian amplitude fluctuations can explain the wide temperature range of the anomalous Nernst signal. The phase fluctuation explanations are based upon the influential work of Emery and Kivelson,³ which preceded the Nernst effect measurements in underdoped cuprates, and the follow-up work of Carlson *et al.*⁵ In this theory, the importance of phase fluctuations is determined by the superfluid density, ρ_s . The smaller the superfluid density, the more significant the phase fluctuations.³ In conventional superconductors, the superfluid density ρ_s is very large.^{3,6} Phase rigidity, or the strength of the phase coherence, is so strong that pairing and long-range order phase coher-

ence occur simultaneously at the transition temperature T_c . The phase degree of freedom plays an insignificant role in determining the transition temperature and other relevant properties. However, in the high- T_c superconductors, with a small superfluid density, the long-range phase coherence is destroyed at T_c while the local Cooper pairing amplitude remains sizable.

Beside the fluctuation theories, many other theories provided possible explanations for the anomalous Nernst effect in hole-doped cuprates.^{7,8,9,10,11,12} However, none of these explanations have gained general acceptance and they are still under debate.

Electron-doped cuprates, $\text{RE}_{2-x}\text{Ce}_x\text{CuO}_{4-\delta}$ (RE=Nd, Pr, Sm), on the other hand, have demonstrated distinctive results. Prior Nernst effect experiments^{13,14,15} in the electron-doped cuprates near optimal doping suggested that electron-doped cuprates are more conventional than their hole-doped counterparts, and that superconducting fluctuations are much weaker, i.e., almost no vortex-like Nernst signal was observed above T_c . In the first part of this paper, a careful study of the vortex Nernst effect in the electron-doped cuprate system $\text{Pr}_{2-x}\text{Ce}_x\text{CuO}_{4-\delta}$ (PCCO) films is reported and the superconducting fluctuation contribution is reexamined. In the underdoped region, we observed a vortex Nernst signal well above T_c , but no such normal state vortex Nernst signal is found in the overdoped region. As in the hole-doped cuprates, we found the stronger superconducting fluctuations in the underdoped PCCO are also compatible with idea of incoherent phase fluctuations.

In the normal state, prior Nernst effect on oxygen-doped $\text{Nd}_{2-x}\text{Ce}_x\text{CuO}_{4-\delta}$ (NCCO) ($x=0.15$) observed a large Nernst signal,^{13,14,15} which has a distinctively different temperature and field dependence from the vortex Nernst signal found in the hole-doped cuprates. The sign change of the Hall coefficient and the enhanced normal state Nernst effect were argued to result from a two-carrier (electron and hole) quasi-particle contribution

around optimal doping of $\text{Ce}=0.15$. This intriguing two-band behavior observed in transport experiments was later confirmed by angle resolved photoemission spectroscopy (ARPES).^{16,17} These measurements found that the Fermi surface (FS) evolves from a Mott insulator parent compound to an electron-like FS centered at $(\pi,0)$ in the underdoped region. At optimal doping, a hole-like FS pocket centered at $(\pi/2, \pi/2)$ coexists with an electron-like pocket near $(\pi, 0)$ and $(0, \pi)$. From the evolution of band structure with doping, one expects a hole-like FS centered at (π, π) in the overdoped region. In fact, Matsui *et al.*¹⁸ recently observed a large hole-like pocket in an overdoped $\text{Nd}_{1.83}\text{Ce}_{0.17}\text{CuO}_4$.

Most of the previous transport measurements were performed on optimally-doped $\text{Nd}_{1.85}\text{Ce}_{0.15}\text{CuO}_{4-\delta}$ and the charge doping was varied by oxygen content. The evolution of these transport properties with oxygen reduction suggested that the hole band is controlled by the oxygen content: a single electron band in the fully oxygenated regime to a two-band regime in the superconducting phase and a hole-like band in the deoxygenated state. Recently, Balci *et al.*¹⁹ observed a large normal state Nernst signal in PCCO films with Ce concentration varied around optimal-doping. This is consistent with previous results in the oxygen-doped NCCO. However, more detailed studies of the Nernst effect in electron-doped cuprates over a wide range of Ce concentration is lacking. It is important to investigate the transport properties in the very underdoped or overdoped regimes since useful information could be obtained for further understanding of the band structure (and scattering) at the extreme dopings. In the second part of this paper, we report our extensive magnetic field driven normal state Nernst effect measurements on $\text{Pr}_{2-x}\text{Ce}_x\text{CuO}_{4-\delta}$ over a wide range of doping ($x=0.05$ to 0.21). We found that the Nernst signal is large around the optimal doping, in agreement with previous reports. In the slightly underdoped and highly overdoped films $x=0.11$ and 0.19 , the Nernst signal is still large. This is contrary to what is expected for a simple single carrier system, suggesting that the transport in this regime may be influenced by anomalous energy dependent scattering at the Fermi surface. For the extremely underdoped $x=0.05$, the Nernst signal decreases rapidly, consistent with a simple single carrier system at this doping.

II. EXPERIMENTS DETAILS

High quality PCCO films with thickness about 2500-3000Å were fabricated by pulsed laser deposition on SrTiO_3 substrates ($10\times 5\text{ mm}^2$).^{20,21} The films were characterized by AC susceptibility, resistivity measurements and Rutherford Back Scattering. The minimum channelling yield obtained was 10% to 20% indicating a good epitaxial growth. A sharp transition ($\Delta T_c < 1\text{ K}$) indicates that our films are of high quality. We note that since the oxygen content has an influence on both the

superconducting and normal state properties of the material,¹³ we optimized the annealing process for each Ce concentration as in Ref.²². The sharp transition, low residual resistivity and the Hall coefficient are exactly the same as the previous report.²² Since the exact content of oxygen cannot be determined in films, we use the low temperature values of the Hall coefficient and Ce content to determine the temperature versus doping phase diagram. The films of size of $10\times 5\text{ mm}^2$ used in Nernst effect experiments were patterned into a standard Hall bar by ion-mill technique.

The Nernst measurements were performed using a one-heater-two-thermometer technique. The film was attached on one end to a copper block with a mechanical clamp and the other end was left free. A small chip resistor heater is attached on the free end, and a temperature gradient is created by applying a constant current to the heater. Two tiny Lakeshore Cernox thermometers are attached on the two ends of the sample to monitor the temperature gradient continuously. The Nernst voltage is measured with a Keithley 2001 multimeter with a 1801 preamp while the field is slowly ramped at a rate of 0.3 T/min between -9 T and $+9\text{ T}$ ($H \perp ab$). The system temperature was well controlled to give stability of the temperature of $\pm 1\text{ mK}$, which enables us to perform a high resolution Nernst voltage measurement (typically $\sim 10\text{ nV}$ in our setup). The temperature gradient is around $0.5\text{-}2\text{ K/cm}$ depending on the temperature of measurement, and the sample temperature is taken as the average of hot and cold end temperatures. The Nernst signal is obtained by subtracting negative field data from positive field data to eliminate any possible thermopower contribution. The Nernst signal was defined as

$$e_y = \frac{E_y}{-\nabla T} \quad (1)$$

where E_y is the transverse electrical field across the sample and $-\nabla T$ is the temperature gradient along its length.

III. VORTEX NERNST EFFECT IN

$$\text{Pr}_{2-x}\text{Ce}_x\text{CuO}_{4-\delta}$$

A. Experimental results

It is known that in a type II superconductor below T_c , vortices moving under a thermal-gradient will generate a transverse electric field, known as the vortex Nernst signal and the sign of the vortex Nernst signal is usually defined as positive.²³ The vortex Nernst signal is usually large compared to the normal state signal. When the temperature is far above T_c , quasi-particles are the only source for a Nernst signal. For a one-carrier system the normal state Nernst effect is much smaller than the vortex Nernst effect.¹

Figure 1 illustrates the vortex Nernst effect and the normal state Nernst signal in an optimally-doped PCCO

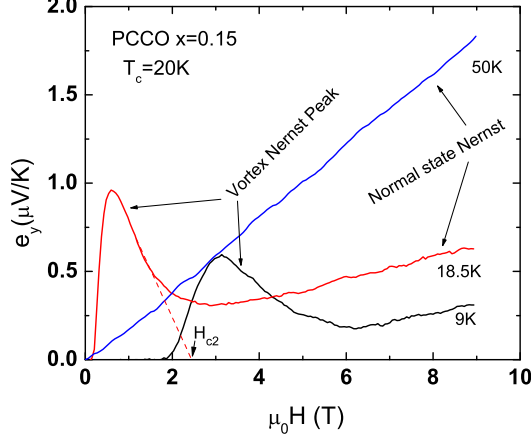


FIG. 1: (color online). Nernst effect in an optimally-doped $x=0.15$ PCCO film at different temperatures.

film. Below T_c and H_{c2} , a sharp and large vortex Nernst peak is seen, which starts from the melting field (the magnetic field at which the vortex is depinned). Above H_{c2} , the Nernst signal is linear in field, as also found when the temperature is above T_c . This linear field dependent Nernst signal is attributed to the normal state quasi-particles. In this figure, we also show a normal state Nernst curve for $T > T_c$ ($T=50$ K). The normal state Nernst signal at $T=50$ K at higher field is even larger than the peak in vortex Nernst signal below T_c . This is in striking contrast to hole-doped cuprates, in which the quasi-particle Nernst signal is much smaller than the vortex Nernst signal.¹ To obtain the net vortex Nernst signal, the linear normal state Nernst signal can be subtracted from the measured data.

We carefully studied the Nernst effect around T_c to search for possible superconducting fluctuation effects in PCCO, especially in the underdoped regime. Fig. 2 shows the low temperature vortex Nernst effect result for an underdoped film $x=0.13$ ($T_c=11.8$ K, from the peak temperature of the imaginary part of susceptibility) after subtraction of the linear normal state Nernst signal. The peak-featured vortex Nernst signal is observed to persist to temperatures higher than T_c . As seen in Fig. 2, the vortex Nernst signal is still robust at $T=17.5$ K, which is about 6 K higher than T_c . When temperature is well above T_c ($T > 20$ K for $x=0.13$), the vortex Nernst signal vanishes and the linear quasi-particle field dependent Nernst signal is recovered. The Nernst effect measurement was also performed on PCCO films with dopings $x=0.14, 0.15, 0.16, 0.17, 0.19$. For $x=0.14$ and $x=0.15$, the result is similar to $x=0.13$, but the onset temperature of the vortex Nernst signal (temperature where a vortex Nernst peak appears) is about 4 K above T_c for $x=0.14$ and 3 K above T_c for $x=0.15$. However, in the overdoped

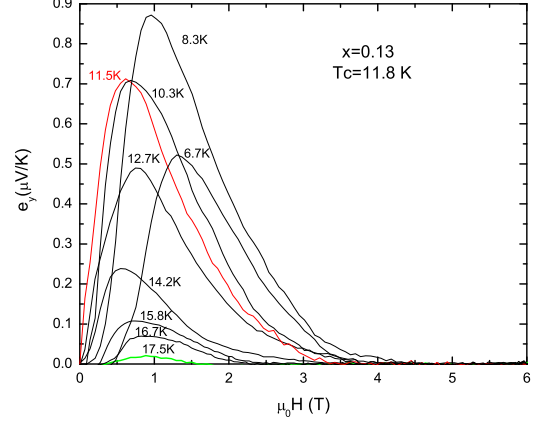


FIG. 2: (color online). Vortex Nernst effect in an underdoped $x=0.13$ PCCO film at different temperatures.

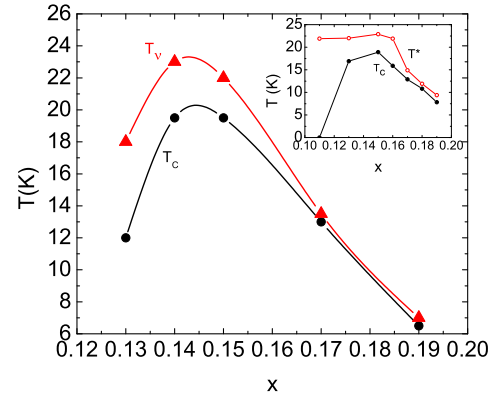


FIG. 3: (color online). Doping dependence of T_c and onset temperature T_v of vortex Nernst signal (error bar is the size of the dot). Inset shows recent planar tunneling data in PCCO.²⁶

films, the vortex Nernst signal (low field peak) vanishes immediately at the superconducting transition temperature T_c . Moreover, the linear quasi-particle Nernst signal emerges when temperature is just above T_c , suggesting that the normal state is recovered, with minimal superconducting fluctuations, right at T_c .

Figure 3 displays the onset temperature of the vortex Nernst signal along with the superconducting transition temperature T_c as a function of doping for PCCO. It is clear that in the underdoped region the difference between these two characteristic temperatures is larger than the overdoped side, suggesting a larger superconducting fluctuation effect in the underdoped region with a more conventional behavior in the overdoped region.

B. Discussion

How do we understand the superconducting fluctuations in the electron-doped cuprates? It is known that superconductivity is characterized by a complex order parameter $|\psi|exp(-i\theta)$, with an amplitude $|\psi|$ and a phase θ at each space point.⁶ Fluctuations in either amplitude or phase will affect the superconducting properties. The conventional fluctuation theories primarily deal with thermal fluctuations of the amplitude $|\psi|$ of the order parameter.^{6,24} By solving the time-dependent Ginzburg-Landau equation in the Gaussian approximation, Ussushkin *et al.*⁴ calculated the transverse thermoelectric coefficient which results from the amplitude fluctuations:

$$\alpha_{xy}^{SC} = \frac{1}{6} \frac{e \xi^2}{\hbar l_B^2} \propto \frac{1}{T - T_c} \quad (2)$$

where α_{xy}^{SC} is the transverse Peltier conductivity, $l_B = (\hbar/eB)^{1/2}$ is the magnetic length and ξ is the in-plane coherence length.

The vortex Nernst signal, $e_y = \alpha_{xy}^{SC}/\sigma_{xx}$ (σ_{xx} is the conductivity), is mainly proportional to the in-plane coherence length ξ_{ab} . In the electron-doped cuprates, the in-plane coherence length increases with doping (H_{c2} decreases rapidly with doping²⁵) and thus from Eq. 2 one would expect a stronger fluctuation effect as doping increases. However, the absence of fluctuation effects in the overdoped PCCO contradicts this theoretical expectation. In addition, compared to the hole-doped cuprates (e.g. LSCO), electron-doped cuprates have a much longer coherence length (about one order of magnitude larger^{19,25}), yet a weaker fluctuation effect is observed: the fluctuation regime, $\Delta T_{fl} = T_\nu/T_c - 1$ is about 0.5 for PCCO with $x=0.13$ and 4 for LSCO with $x=0.1$ ($T_c=20$ K).¹ These two results strongly suggest that conventional amplitude fluctuation theory can not explain the Nernst effect results in underdoped electron-doped cuprates.

Now we turn to phase fluctuations, which are claimed to explain the anomalous Nernst effect in the hole-doped cuprates. In conventional superconductors, phase fluctuations plays an insignificant role in determining the transition temperature because of the large superfluid density ρ_s . However, in the high- T_c superconductors, the proximity to the Mott insulator leads to a very small superfluid density. Therefore, it is possible that long-range phase coherence is destroyed at T_c while the local Cooper pairing amplitude remains sizable. The significance of the phase fluctuation can be assessed by evaluating the phase stiffness temperature,³ $T_\theta^{max} = A\rho_s(0)d/m^*$, at which phase order would disappear (here d the spacing between adjacent CuO_2 layers, $A=0.9$ is a numeric factor for quasi-2D systems and m^* the effective mass). If $T_c \ll T_\theta^{max}$, phase fluctuations are relatively unimportant, and T_c will be close to the mean-field transition temperature, T_c^{MF} , as predicted by BCS theory.

On the other hand, if $T_\theta^{max} \approx T_c$, then T_c is determined primarily by phase ordering, and T_c^{MF} is simply the characteristic temperature below which pairing becomes significant locally. In conventional superconductors, T_θ^{max} is orders of magnitude larger than T_c , and phase coherence is so strong that T_c is the Cooper pair formation temperature. In the overdoped hole-doped cuprates, T_θ^{max}/T_c is around 2-5, suggesting that phase fluctuations become more important. In the underdoped hole-doped cuprates, T_θ^{max} is very close to T_c , suggesting that phase fluctuations are dominant in determining the superconducting phase transition. The fluctuations suppress the transition temperature from the mean-field value T_c^{MF} , at which Cooper pairs form, to the observed T_c where long-range phase coherence is established. In the electron-doped cuprate PCCO, penetration depth measurements gave $\lambda^{-2}(0)=9, 15$ and $40 \mu\text{m}^{-2}$ for $x=0.13, 0.15$ and 0.17 respectively.²⁷ Using the relation $\rho_s(0) = m^*/e^2\lambda^2(0)$, we can estimate the T_θ^{max}/T_c value for PCCO. Simple calculation gives $T_\theta^{max}/T_c=2, 2.4$ and 11 for $0.13, 0.15$ and 0.17 respectively. Thus, phase fluctuations are suppressed in the overdoped region since $\frac{T_\theta^{max}}{T_c} \gg 1$ and then $T_c \approx T_c^{MF}$. Although the values of T_θ^{max}/T_c of the underdoped and optimally-doped PCCO are close to those of optimally-doped and overdoped LSCO, the fluctuation regime is somewhat narrower in PCCO than LSCO ($\Delta T_{fl}=0.5\pm0.1$ for PCCO with $x=0.13, 1.2\pm0.1$ for LSCO $x=0.17$).¹ A likely reason is the weaker coupling of the Cooper pairs in the electron-doped cuprates. The pairing amplitude measured by the superconducting gap is about 3.5 meV for PCCO $x=0.13$, smaller than the gap value (~ 10 meV) for the optimally doped LSCO.²⁸ The value of $2\Delta/k_B T_c$ is smaller in PCCO (~ 3.5) than in LSCO (~ 8). This suggests that the temperature driven pair-breaking effect is stronger in PCCO, so that any local pairing can not survive with increasing temperature. Thus, the thermal pair breaking competes with the phase fluctuation effect and reduces the size of the fluctuation region.

In addition, our resistivity measurements on the underdoped and optimally-doped PCCO films also show some interesting results. As displayed in Fig. 4, the blue curves are the zero-field resistivity of $x=0.13$ and 0.15 . In order to eliminate the negative magnetoresistance at these dopings, we measured the in-plane resistivity versus field at different temperatures and extrapolated the data to get the “effective” zero-field normal state resistivity. Its temperature dependence is shown as red curve in Fig. 4. The arrows mark the temperature where the zero-field resistivity deviates from the zero-field normal state resistivity. Interestingly, the onset temperature of the deviation is slightly higher than the onset temperatures of the vortex Nernst effect in both underdoped and optimally-doped samples. Although the excessive conductivity (paraconductivity) is usually attributed to amplitude fluctuations,²⁴ this is not certain in PCCO case because phase fluctuations could also induce the enhanced conductivity above T_c . However, to distinguish

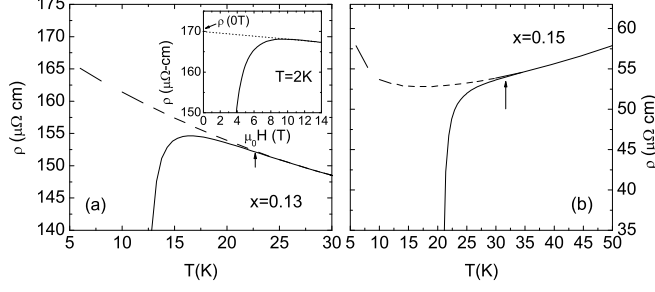


FIG. 4: Paraconductivity of the underdoped $x=0.13$ (a) and optimally-doped $x=0.15$ (b) PCCO films. Inset shows the procedure of obtaining the zero-field normal state resistivity [dashed lines in (a) and (b)].

these fluctuations is difficult theoretically and experimentally and it is beyond our knowledge and the scope of this paper.

We mention that a planar tunneling experiment in PCCO observed a normal state energy gap throughout the entire doping range.²⁶ This normal state gap persists to a temperature higher than the superconducting transition temperature T_c in the underdoped region but follows T_c on the overdoped side (inset of Fig. 3). This was interpreted as a result of finite pairing amplitude above T_c in the underdoped region. The onset temperature of the vortex Nernst signal extends well into this region, suggesting that may be related to the normal state gap seen the tunneling.

C. Conclusion

To summarize this part, we carefully investigated the superconducting fluctuation effects in PCCO films by Nernst effect measurements. We found that the fluctuations are stronger in the underdoped region than in the overdoped region. We argued against amplitude fluctuations as an explanation of this observation. It is likely that phase fluctuations are responsible for the normal state vortex signal in the underdoped PCCO films. This is consistent with the anomalous Nernst effect found in the hole-doped cuprates.

IV. NORMAL STATE NERNST EFFECT IN

$$Pr_{2-x}Ce_xCuO_{4-\delta}$$

A. Experimental results

Electron-doped cuprates are distinct from hole-doped cuprates in having a low H_{c2} and thus the normal state can be easily accessed for temperature below T_c . As

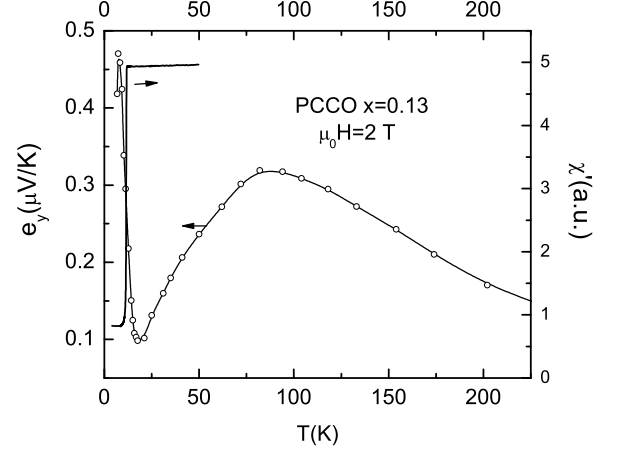


FIG. 5: Temperature dependence of the Nernst signal in an underdoped PCCO with $x=0.13$ at $\mu_0 H=2$ T. The $H_{c2}(0)$ of this film is about 7 T and T_c is 11.8 K. Solid line is the real part of the zero-field AC susceptibility.

shown before, when the external magnetic field is larger than H_{c2} or temperature higher than T_c , the Nernst signal e_y in PCCO is linear in field. The Nernst coefficient ν is defined as the slope of $e_y(B)$, i.e., $\nu \equiv e_y/B$.

Before showing all the normal state Nernst effect data, let us first compare the vortex Nernst signal ($T < T_c$) and the normal state ($T > T_c$) for $H=2$ T in an underdoped $x=0.13$ film. As shown in Fig. 5, two peaks are prominent in the temperature dependence of the Nernst signal. The lower temperature peak is produced by vortex motion in the superconducting state and the higher temperature peak is from the normal state quasi-particles. In strong contrast to the Nernst effect in hole-doped cuprates,¹ the normal state Nernst signal is much larger and its magnitude is comparable to the vortex Nernst signal. As the field approaches H_{c2} , the vortex Nernst signal decrease quickly, but the normal state signal increases linearly, as seen in Fig. 1. In the following, the normal state Nernst signal is taken at $H=9$ T, which is greater than $H_{c2}(0)$ for all the PCCO films.

Although our focus of interest is the Nernst effect at the doping extremes, we measured the normal state Nernst effect on PCCO films systematically throughout the entire doping range, from the extremely underdoped ($x=0.05$) to the highly overdoped ($x=0.21$). Fig. 6 shows the temperature dependence of the normal state Nernst signal e_y for all the doped PCCO films. The Nernst signal increases as temperature decreases, reaches a peak at a certain temperature then decreases linearly towards zero as $T \rightarrow 0$. The magnitude of the Nernst signal and its temperature dependence are rather similar for all the dopings except the extremely underdoped $x=0.05$. The linear temperature dependence of the the Nernst signal below the peak temperatures is as predicted for quasi-

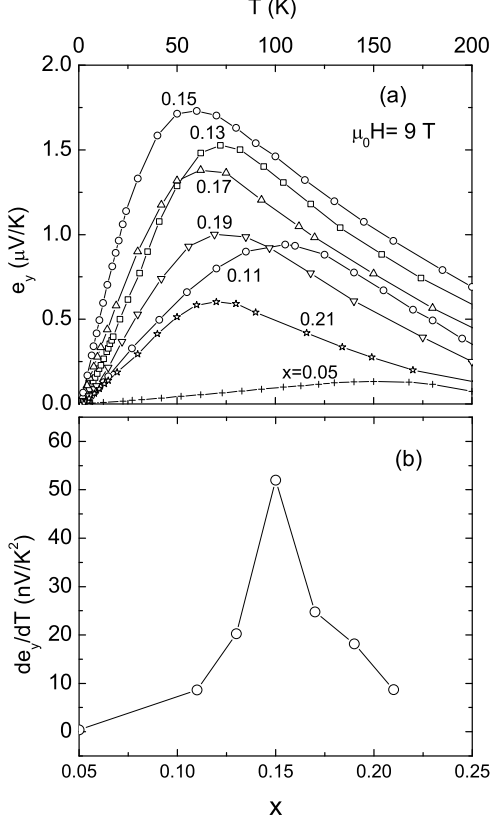


FIG. 6: (a) Temperature dependence of normal state Nernst signal at $\mu_0 H = 9$ T for all the doped PCCO films, (b) Doping dependence of the initial slope of the Nernst signal curves in (a) at low temperatures.

particles (see later discussion). In Fig. 6(b), the doping dependence of the slope (de_y/dT) of the low temperature Nernst signal is shown. We see that de_y/dT has a maximum at the optimal doping and decreases rapidly with underdoping and overdoping.

B. Discussion

One-band transport

The anomalously large normal state Nernst effect that we observed throughout almost the entire doping range strongly contrasts with the hole-doped cuprates and with normal metals in which the magnitude of the Nernst signal is in the order of nV/K . To understand this, we attempted a simple comparison with conventional theories for a one-band (single-carrier) system. Within Boltz-

mann theory, the Nernst coefficient can be expressed as²⁹,

$$\nu = \frac{\pi}{3} \frac{k_B^2 T}{eB} \frac{\partial \tan \theta_H}{\partial \epsilon} = \frac{\pi^2 k_B^2 T}{3m^*} \frac{\partial \tau}{\partial \epsilon} \Big|_{\epsilon_F} \quad (3)$$

where $\tan \theta_H$ is the Hall angle and τ the scattering time. Eq. 3 shows that the Nernst signal is linearly dependent on the temperature and our low temperature data at all dopings is consistent with this prediction. To estimate the magnitude of the low temperature Nernst signal, we can replace $\frac{\partial \tau}{\partial \epsilon_F}$ with $\frac{\tau}{\epsilon_F}$ by assumption of a weak energy dependence of τ at the Fermi energy ϵ_F . This gives⁴¹

$$e_y = \nu B = 283 \omega_c \tau \frac{k_B T}{\epsilon_F} \mu\text{V/K}, \quad (4)$$

where $\omega_c = eB/m^*$ is the cyclotron frequency and m^* is the electron mass. Eq. 4 suggests that the Nernst signal is proportional to $\omega_c \tau$ and inversely proportional to Fermi energy.

For a single carrier system, $\omega_c \tau$ can be estimated from the residual resistivity ρ_0 and the carrier density n , i.e., $\omega_c \tau = B/\rho_0 n e$ (which is equivalent to $\omega_c \tau = \tan \theta_H$). For the optimally-doped $x=0.15$, normal state resistivity measurement gives $\rho_0 = 57 \mu\Omega\text{cm}$. The estimate of the carrier density n is rather unclear. For comparison, we estimate n in two different ways. From the Hall coefficient,²² one gets $n_{Hall} = \frac{1}{R_H(0)e} = 4.2 \times 10^{21}/\text{cm}^3$ and then $\omega_c \tau = 0.022$ at 9 T. Another way is by assuming 0.15 electron/unit cell, $n_{cell} = \frac{0.15}{3.95^2 \times 6} \text{\AA}^{-3} = 1.58 \times 10^{21}/\text{cm}^3$, which yields $\omega_c \tau = 0.059$. The Fermi energy ϵ_F can be obtained from ARPES^{16,34} where $\epsilon_F \sim 0.61$ eV (using the Fermi wave number $k_F \sim 0.7\pi/a$ and $\epsilon_F = \frac{\hbar^2 k_F^2}{2m^*}$) and thus $\epsilon_F/k_B \approx 7100$ K. Inserting these numbers into the expression for e_y in Eq. 4, we find $de_y/dT = 1.0$ nV/K² (from n_{Hall}) and 1.8 nV/K² (from n_{cell}). These values are more than one order of magnitude smaller than the measured value of 53 nV/K² [see Fig 6(b)].

Now we apply this estimation to the overdoped sample. The numbers for $x=0.19$ are $\rho_0 = 20 \mu\Omega\text{cm}$, $n_{Hall} = 6.5 \times 10^{21}/\text{cm}^3$ and $n_{cell} = 2.01 \times 10^{21}/\text{cm}^3$; $\omega_c \tau$ then is 0.04 and 0.139 respectively for $H=9$ T. Although the Fermi energy of $x=0.19$ is still unknown, we find from ARPES experiments¹⁸ that $k_F \sim 0.7\pi/a$ remains nearly the same for x from 0.15 to 0.17. Therefore, we expect that ϵ_F should also be approximately 7100 K at $x=0.19$. Plugging these numbers into Eq. 4, we get $de_y/dT = 1.6$ nV/K² and 5.6 nV/K² for n_{Hall} and n_{cell} respectively. If we estimate the carrier density from the area of the Fermi pockets of $x=0.19$ obtained from ARPES¹⁸ and the spin-density-wave (SDW) calculation,³² we get $n_{FS} = 4.3 \times 10^{21}/\text{cm}^3$. This yields $de_y/dT \sim 2.5$ nV/K². All these estimated values are smaller than the measured value of 20 nV/K² for $x=0.19$.

The large difference of these simple estimates from our experiments shows that a conventional one-band model is not applicable to PCCO, even in the highly overdoped region with a large hole-like FS. This suggests that there may be an unusual energy dependent scattering at the FS which enhances Eq. 3 over our simple assumption above.

Two-band transport

The sign change and the temperature dependence of both Hall coefficient²² and thermopower,³⁶ the anomalously large Nernst signal and magnetoresistance (to be shown next) can not be explained by a one-band model. Therefore, one has to consider a two-carrier transport model for the electron-doped cuprates.

We start with an estimation of the Nernst signal within a two-band Boltzmann framework. In this model, assuming an identical relaxation for both electron and hole carriers, Oganensyan²⁹ found that the Nernst signal is maximal when the bands are exactly compensated ($n_h = n_e$) and the expression of the Nernst signal becomes

$$e_y = B\nu = \frac{2\pi^2}{3} \frac{k_B^2 T \tau}{e\hbar} \frac{1}{(k_F \ell_B)^2} \quad (5)$$

Inserting $k_F \sim 0.5 \text{ \AA}^{-1}$ obtained from ARPES experiments^{16,34} and $\tau \sim 4.16 \times 10^{-13} \text{ s}$ from optics ($1/\tau = 80 \text{ cm}^{-1}$ for T just above T_c)³⁵ for PCCO $x=0.15$, we get $de_y/dT \sim 25 \text{ nV/K}^2$ for $\mu_0 H = 9 \text{ T}$. This simple estimation is slightly smaller than the measured value of $53 \text{ } \mu\text{V/K}^2$, but suggests that this two-band Boltzmann model could explain the Nernst effect in PCCO.

The enhanced Nernst effect in a two-band system can be easily understood from the expressions for the Nernst signal and thermopower (Ref.³³),

$$e_y = S \left(\frac{\alpha_{xy}^h + \alpha_{xy}^e}{\alpha_{xx}^h + \alpha_{xx}^e} - \frac{\sigma_{xy}^h + \sigma_{xy}^e}{\sigma_{xx}^h + \sigma_{xx}^e} \right) \quad (6)$$

$$= S(\tan\theta_T - \tan\theta_H) \quad (7)$$

and

$$S = \frac{\alpha_{xx}^h + \alpha_{xx}^e}{\sigma_{xx}^h + \sigma_{xx}^e} \quad (8)$$

here h and e denote the hole and electron bands. Considering the charge carrier symmetry, $\sigma_{xy}^h = -\sigma_{xy}^e$ and $\alpha_{xy}^h = \alpha_{xy}^e$, the second term in Eq. 6 will vanish and the first term will be enhanced. Meanwhile, the counterflow of carriers with different sign in Eq. 7, i.e., $\alpha_{xx}^h = -\alpha_{xx}^e$, will lead to a small thermopower. Thus, in PCCO, the enhanced Nernst signal and small thermopower near optimal doping supports the two-band model. For the underdoped $x=0.13$ and 0.11 , a larger thermopower is found³⁶ and the Nernst signal is still large. This could be due to a contribution from the emerging hole band, as found in the ARPES experiments.^{16,18}

The small thermopower³⁶ and sizable Nernst signal (comparable to the optimal doping) in the overdoped $x=0.19$ also suggests a possible two-band contribution. However, this appears to be incompatible with the single large hole pocket seen in ARPES.¹⁸ To explore this further, we look at $\text{Stan}\theta_H$ obtained from the thermopower³⁶ and the Hall angle measurements,³⁰ for all the doped PCCO films. As seen in Fig. 7, $\text{Stan}\theta_H$ decreases with increasing doping and its magnitude is much

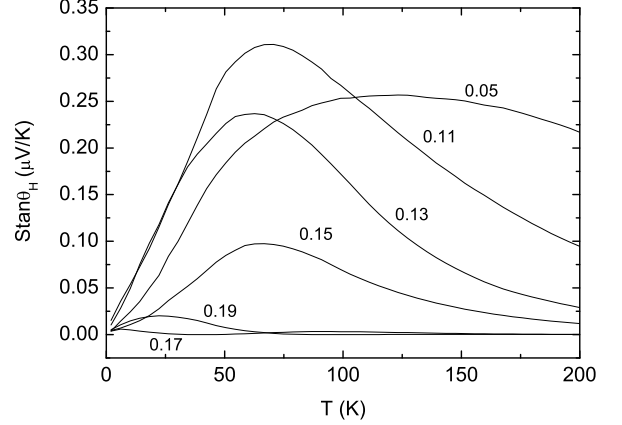


FIG. 7: Temperature dependence of $\text{Stan}\theta_H$ of PCCO films at $\mu_0 H = 9 \text{ T}$.

smaller than the Nernst signal in Fig. 6 for all the dopings except the extremely underdoped $x=0.05$. As we just described, to have a large Nernst signal, the difference between $\text{Stan}\theta_H$ (the second term in Eq. 7) and $\text{Stan}\theta_T$ (the first term in Eq. 7) has to be large. In PCCO, the large difference in the magnitude of e_y and $\text{Stan}\theta_H$ (see Fig. 6 and Fig. 7) suggests a large thermal Hall angle θ_T (recall that S is small). Therefore, the large value of $\tan\theta_T$ indicates a two-carrier contribution. This is also seen in the overdoped PCCO from Fig. 6 and Fig. 7, strongly suggesting the incompatibility with the single hole-like FS expectation. Note, for a single carrier system, such as the extremely underdoped $x=0.05$ PCCO, the small Nernst signal is comparable to $\text{Stan}\theta_H$, suggests a negligible $\text{Stan}\theta_T$. It is worth mentioning that two-band transport in the highly overdoped PCCO is also consistent with the high-field nonlinear Hall resistivity.³⁷

We have shown that the anomalous large Nernst effect and small $\text{Stan}\theta_H$ in the overdoped PCCO films are qualitatively consistent with a two-band model. However, this is contrary to the ARPES experiments,¹⁸ in which a simple hole-like Fermi pocket is found for doping $x \geq 0.17$. Another possible reason for the enhanced Nernst signal, as indicated in Eq. 3, could be a strong anisotropic energy dependence of the scattering $\tau(\epsilon_F)$ at the Fermi surface. The remanent contribution of “hot spots” near the $(\pi/2, \pi/2)$ region to the Nernst signal could be dominant even in the overdoped regime.

The magnetoresistance in a two-carrier system is closely related to the Nernst effect. From Eq. 6 and 8, one can rewrite the Nernst coefficient as³⁸:

$$\nu = \frac{\nu_h \sigma_h + \nu_e \sigma_e}{\sigma} + \frac{\sigma_h \sigma_e (S_h - S_e)(\sigma_h R_h - \sigma_e R_e)}{\sigma^2} \quad (9)$$

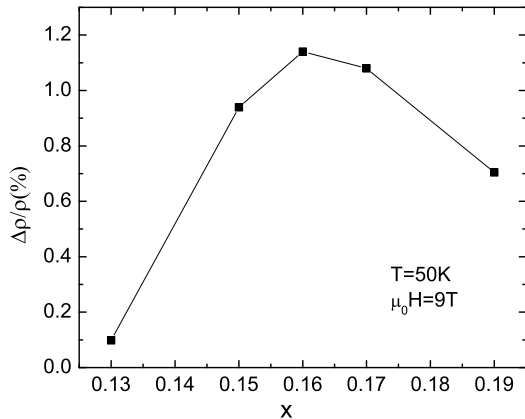


FIG. 8: Doping dependence of the normal state magnetoresistance in PCCO films at $T=50$ K (T is set at 50 K in order to avoid the low temperature superconducting fluctuations).

The magnetoresistance for a two-band system is¹⁵

$$\frac{\Delta\rho}{\rho} = \frac{\sigma_h\sigma_e(\sigma_h R_h - \sigma_e R_e)^2 B^2}{\sigma^2} \quad (10)$$

The second term of Eq. 9 is responsible for the potentially larger Nernst signal with respect to a single carrier system. The factor $(\sigma_h R_h - \sigma_e R_e) = (\mu_h - \mu_e)$ can reach a maximum value if the mobilities are large and $\mu_h = -\mu_e$, which will lead to an enhanced Nernst signal. From Eq. 10, we can identify the same mobility coefficient, $(\sigma_h R_h - \sigma_e R_e)$, found in the Nernst coefficient. This indicates that a maximum of the magnetoresistance is likely to coincide with a maximum of the Nernst coefficient as the doping and the mobilities change.^{13,15} In Fig. 8, we show the magnetoresistance at 50 K as a function of Ce content. We see that the transverse magnetoresistance is large and positive (compared to the magnetoresistance in the p-doped cuprates, which is one order of magnitude smaller) for all the superconducting films. The maximum magnetoresistance occurs around optimal doping, at which doping, the Nernst signal [Fig. 6(b)] also reach a maximum. The strong correlation between Nernst effect and the magnetoresistance strongly suggests that PCCO is a two-band system for dopings in the superconducting dome region of the phase diagram.

Finally, we discuss the higher temperature peak feature that found in the temperature dependence of the Nernst signal [Fig. 5(a)]. A similar peak feature was found in thermopower measurements which suggests a common origin. A prior work³⁹ proposed that the ther-

moelectric power of the underdoped hole-doped cuprates could reveal the opening of a pseudogap. The pseudogap increases the thermopower leading to a broad maximum above T_c but below T^* . For the PCCO system, we also observed a maximum thermopower at fairly high temperature (between 50 K and 100 K) with respect to T_c in the underdoped region. It is possible that the thermopower is influenced by the high temperature gap found in the optics and ARPES measurements⁴⁰. The transverse thermoelectric effect, i.e., Nernst effect, also presents a broad higher temperature peak in the entire doping range. The peak feature could also be a result of the influence of the high energy gap and fluctuations in the overdoped region. Further understanding of this will require future study.

The peak feature in the temperature dependence of the Nernst signal could also be a result of a phonon-drag effect. As proposed by Behnia *et al.*⁴¹ for Bismuth, in the Ettingshausen geometry (transverse temperature gradient generated by external magnetic field when a longitudinal electrical current is present), when electrons interact with phonons, the electric current gives rise to an entropy current of phononic origin, and a significant Ettingshausen effect. Since the Onsager relation ties the amplitudes of the Ettingshausen and Nernst effects, this implies that the Nernst effect should also be enhanced. However, the application of this model to the PCCO case is not clear at this time and future work is required.

C. Conclusion

We performed measurements of the magnetic field driven normal state Nernst effect on electron-doped cuprate $\text{Pr}_{2-x}\text{Ce}_x\text{CuO}_{4-\delta}$ films over a wide range of doping and temperature. We find an anomalously large Nernst signal near optimal doping, which is consistent with prior reports. More interestingly, the Nernst signal is still large in the highly overdoped films and the slightly underdoped films. This can not be explained by a single-band model, and a two-band model has to be considered. The qualitative consistence between the experimental transport data and the two-band model for the overdoped films, which appears inconsistent with ARPES experiments, will require further research.

Acknowledgments

We thank A. Millis, K. Behnia, V. Yakovenko, W. Yu, V. Oganessian and H. Kontani for fruitful discussions. P.L. thanks H. Balci for the Nernst effect measurements. We acknowledge the support of NSF under Grant DMR-0352735.

* Electronic address: pcl@physics.umd.edu

¹ Y. Wang, L. Li, and N. P. Ong, Phys. Rev. B **73**, 024510

- (2006) and references therein.
- ² Z. Xu, N.P. Ong, Y. Wang, T. Kakeshita, and S. Uchida, *Nature(London)* **406**, 486 (2000).
 - ³ V. J. Emery and S. A. Kivelson, *Nature(London)* **374**, 434 (1995).
 - ⁴ I. Ussishkin and S. L. Sondhi, *Int. J. Mod. Phys. B* **18**, 3315 (2004); I. Ussishkin, S. L. Sondhi, and D. A. Huse, *Phys. Rev. Lett.* **89**, 287001 (2002).
 - ⁵ E. W. Carlson, V. J. Emery, S. A. Kivelson, and D. Orgad, *The Physics of Conventional and Unconventional Superconductors* ed. K. H. Bennemann and J. B. Ketterson (Springer-Verlag); cond-mat 0206217 (2002).
 - ⁶ M. Tinkham, *Introduction to Superconductivity*, 2nd ed. (McGraw-Hill, New York, 1996).
 - ⁷ H. Kontani, *Phys. Rev. Lett.* **89**, 237003 (2002).
 - ⁸ S. Tan and K. Levin, *Phys. Rev. B* **69**, 064510 (2004).
 - ⁹ C. Honerkamp and P. A. Lee, *Phys. Rev. Lett.* **92**, 177002 (2004).
 - ¹⁰ R. Ikeda, *Phys. Rev. B* **66**, 100511(R), (2002).
 - ¹¹ A. S. Alexandrov and V. N. Zavaritsky, *Phys. Rev. Lett.* **93**, 217002 (2004).
 - ¹² P. W. Anderson, *Phys. Rev. Lett.* **96**, 017001 (2006)
 - ¹³ Wu Jiang, S. N. Mao, X. X. Xi, Xiuguang Jiang, J. L. Peng, T. Venkatesan, C. J. Lobb, and R. L. Greene, *Phys. Rev. Lett.* **73**, 1291 (1994).
 - ¹⁴ F. Gollnik and M. Naito, *Phys. Rev. B* **58**, 11734 (1998).
 - ¹⁵ P. Fournier, X. Jiang, W. Jiang, S. N. Mao, T. Venkatesan, C. J. Lobb, and R. L. Greene, *Phys. Rev. B* **56**, 14149 (1997).
 - ¹⁶ N. P. Armitage, F. Ronning, D. H. Lu, C. Kim, A. Damascelli, K. M. Shen, D. L. Feng, H. Eisaki, Z.-X. Shen, P. K. Mang, N. Kaneko, M. Greven, Y. Onose, Y. Taguchi, and Y. Tokura, *Phys. Rev. Lett.* **88**, 257001 (2002).
 - ¹⁷ H. Matsui, K. Terashima, T. Sato, T. Takahashi, S.-C. Wang, H.-B. Yang, H. Ding, T. Uefuji, and K. Yamada, *Phys. Rev. Lett.* **94**, 047005 (2005); H. Matsui, K. Terashima, T. Sato, T. Takahashi, M. Fujita, and K. Yamada, *Phys. Rev. Lett.* **95**, 017003 (2005).
 - ¹⁸ H. Matsui, T. Takahashi, T. Sato, K. Terashima, H. Ding, T. Uefuji, and K. Yamada, *Phys. Rev. B* **75**, 224514 (2007).
 - ¹⁹ H. Balcı, C. P. Hill, M. M. Qazilbash, and R. L. Greene, *Phys. Rev. B* **68**, 054520 (2003).
 - ²⁰ E. Maiser, P. Fournier, J.-L. Peng, F. M. Araujo-Moreira, T. Venkatesan, R. L. Greene, and G. Czjzek, *Physica C* **297**, 15 (1998).
 - ²¹ J. L. Peng, E. Maiser, T. Venkatesan, R. L. Greene, and G. Czjzek, *Phys. Rev. B* **55**, R6145 (1997).
 - ²² Y. Dagan, M. M. Qazilbash, C. P. Hill, V. N. Kulkarni, and R. L. Greene, *Phys. Rev. Lett.* **92**, 167001 (2004).
 - ²³ N. P. Ong, Y. Wang, S. Ono, Y. Ando, and S. Uchida, *Annalen der Physik(Leipzig)* **13**, 9 (2004).
 - ²⁴ A. I. Larkin and A. A. Varlamov, *The Physics of Superconductors, Vol 1: Conventional and High-Tc Superconductors* (Springer, Berlin, 2003).
 - ²⁵ P. Fournier and R. L. Greene, *Phys. Rev. B* **68**, 094507 (2003).
 - ²⁶ Y. Dagan, M. M. Qazilbash, and R. L. Greene, *Phys. Rev. Lett.* **94**, 187003 (2005).
 - ²⁷ A. Snezhko, R. Prozorov, D. D. Lawrie, R. W. Giannetta, J. Gauthier, J. Renaud, and P. Fournier, *Phys. Rev. Lett.* **92**, 157005 (2004).
 - ²⁸ A. Ino, C. Kim, M. Nakamura, T. Yoshida, T. Mizokawa, A. Fujimori, Z.-X. Shen, T. Kakeshita, H. Eisaki, and S. Uchida, *Phys. Rev. B* **65**, 094504 (2002).
 - ²⁹ V. Oganessian and I. Ussishkin, *Phys. Rev. B* **70**, 054503 (2004).
 - ³⁰ Y. Dagan and R. L. Greene, *Phys. Rev. B* **76**, 024506 (2007).
 - ³¹ V. Z. Kresin and S. A. Wolf, *Phys. Rev. B* **41**, 4278 (1990).
 - ³² J. Lin and A. J. Millis, *Phys. Rev. B* **72**, 214506 (2005).
 - ³³ Romain Bel, Kamran Behnia, and Helmuth Berger, *Phys. Rev. Lett.* **91**, 066602 (2003).
 - ³⁴ T. Sato, T. Kamiyama, T. Takahashi, K. Kurahashi, and K. Yamada, *Science* **291**, 1517 (2001).
 - ³⁵ C. C. Homes, R. P. S. M. Lobo, P. Fournier, A. Zimmers, and R. L. Greene, *Phys. Rev. B* **74**, 214515 (2006).
 - ³⁶ Pengcheng Li, K. Behnia and R. L. Greene, *Phys. Rev. B* **75**, 020506(R) (2007).
 - ³⁷ Pengcheng Li, F. F. Balakirev, and R. L. Greene, *Phys. Rev. Lett.* **99**, 047003 (2007).
 - ³⁸ R. Bel, Ph.D thesis, ESPCI, Paris, France (2004).
 - ³⁹ J. L. Tallon, J. R. Cooper, P. S. I. P. N. de Silva, G. V. M. Williams, and J. W. Loram, *Phys. Rev. Lett.* **75**, 4114 (1995).
 - ⁴⁰ A. Zimmers, J. M. Tomczak, R. P. S. M. Lobo, N. Bonetemps, C. P. Hill, M. C. Barr, Y. Dagan, R. L. Greene, A. J. Millis, and C. C. Homes, *Europhys. Lett.* **70**, 225 (2005).
 - ⁴¹ Kamran Behnia, Marie-Aude Measson, and Yakov Kopelevich, *Phys. Rev. Lett.* **98**, 076603 (2007).